# KA-BAND CHOKE-RING HORN TT&C ANTENNAS COMBINING CONVENTIONAL MILLING AND ALUMINUM SELECTIVE LASER MELTING (SLM) MANUFACTURING

C. Stoumpos<sup>(1)</sup>, N. J. G. Fonseca<sup>(1)</sup>, G. Branger<sup>(1)</sup>, Q. Lamotte<sup>(1)</sup>, M. Romier<sup>(1)</sup>, N. Capet<sup>(1)</sup>, R. Fragnier<sup>(2)</sup>

(1)Anywaves Bât Toulouse 2000, 2 Esp. Compans Caffarelli Hall D, 31000, Toulouse, France Email: h.stoumpos@anywaves.com

(2) Centre National d'Études Spatiales (CNES), Antennas Department 18 Av. Edouard Belin, 31400 Toulouse, France Email: Remi.Fragnier@cnes.fr

Abstract - This paper presents the results of an R&T activity led by Anywaves with the support of CNES on Ka-band choke-ring horn antennas for future Telemetry, Tracking and Control satellite applications. Two metal-only antenna topologies operating in the frequency band 29.5~30 GHz have been designed and optimised for hemispherical coverage radiation patterns. Two prototypes, using only conventional milling for the first and a combination of conventional milling and selective laser melting for the second antenna, have been fabricated and tested so that the numerically calculated RF performance of the antennas can be validated. On-platform simulations have also been performed so as to characterise the sensitivity of the radiation patterns of the antennas.

#### I. INTRODUCTION

In Low Earth Orbit (LEO) constellations, low-gain antennas (LGAs) with hemispherical coverage radiation patterns are essential in Telemetry, Tracking and Control (TT&C) satellite sub-systems to secure a communication link with the satellite independently of its altitude [1]. This is important in the early phase of the in-orbit deployment, but also when the altitude and orbit control is lost. Ka-band is emerging as an alternative to the S- band frequencies broadly used in TT&C subsystems. Typical requirements of TT&C satellite subsystems include low RF losses, high power-handling, relatively high Cross-Polar Discrimination (XPD) levels, high Front-to-Back Ratio (FTBR), on-platform radiation pattern stability (i.e., low sensitivity against the presence of a ground plane), as well as robust mechanical and thermal behaviour.

Antenna elements that can provide hemispherical coverage or isoflux radiation patterns are cross-dipole antennas [2]-[3], dielectric resonator antennas [4], patch antennas [5]-[6], dielectric lens loaded antennas [7], conformal printed dipole antennas [8], helical antennas [9]-[12], anisotropic metasurface antennas [13], subreflector-based waveguide choke-ring antennas [14], dielectric-loaded waveguide choke-ring antennas [15] and waveguide choke-ring antennas [16]-[19]. For space

applications, choke-ring horn antennas and low-gain helix antennas are the most appealing candidates owing to their robust RF performance and relatively simple structure. Helix antennas present a smaller footprint, and they are typically preferred when multipath is not of primal importance. On the contrary, choke-ring horn antennas present lower losses in higher frequencies (waveguide-based solution) as well as a sharper roll-off and low back-lobe radiation levels. The latter feature makes this type of antenna more immune against the presence of the platform which can act as a large ground plane as well as against scatterers which are likely to cause multipath interference. In other words, owing to its electrically large footprint, choke-ring horn antennas present high radiation pattern stability when placed on satellite platforms.

Choke-ring horn antennas belong to the family of primary feeds suitable for sectoral pattern synthesis and, as a result, are widely known for their robust performance and their ability to fulfil to a good extent the above requirements [20]. Given the fact that chokering antennas present diameters of several wavelengths, the main advantage for Ka-band solutions relates to the small footprint of RF hardware owing to the small operating wavelength. Broader absolute bandwidths compared to lower frequencies are also considered.

Additive manufacturing techniques employing metallic powder, such as Selective Laser Melting (SLM), have been proven to be disruptive and affordable solutions as far as antennas and RF hardware are concerned [21]. The rapid evolution of this manufacturing process and its acceptability for space qualified products within the ECSS framework has paved new ways of designing and developing waveguide-based solutions and, in many cases, this comes to a lower overall cost. The fabrication precision remains, of course, an open challenge and a particularly critical component where high-frequency hardware is concerned. Several axially corrugated (choke-ring type) [15], [22]-[26] and longitudinally corrugated] horn antennas [27]-[29] in various frequency bands can be found in the literature over the recent years, a fact that denotes an increasing trend on the 3D-printing of such type of antenna elements.

In this paper, we present two low-cost, flat-top (hemispherical) pattern choke-ring antennas; one in conventional milling and one in additive manufacturing. The design and optimization as well as the measurement results of the two solutions are also shown and discussed. Last, we present simulation results of onplatform analyses assuming the antennas on nanosatellites in order to monitor the pattern stability and the influence of realistic platform environments on the antennas' radiation. This study allowed us to compare the two manufacturing methods on specific criteria such as the cost and industrialization axes.

#### II. SPECIFICATIONS AND ANTENNA DESIGN

The CAD models of the two choke-ring horn antennas are depicted in Fig. 1, with Fig. 1(a) showing the perspective back and front view of the antenna designed for conventional manufacturing and Fig. 1(b) the perspective back and front view of the antenna designed for hybrid manufacturing, namely, the choke-ring horn part was fabricated in additive manufacturing and the septum feeder in milling (i.e., the two antennas have the same microwave device as excitation network).

The antennas were optimized using TICRA's CHAMP 3D software [30], which employs mode matching to solve for fields in the interior region of the horn and BoR-MoM for the exterior region. A 2-stage optimization approach was employed. First, a genetic algorithm was used to optimize the antenna's performance while a gradient algorithm was employed to fine-tune the antenna at the end. The optimization of choke-ring horn antennas is highly dependent on the initial radiation pattern; the one occurring by the feeding waveguide. The requirement is the least possible directive radiation pattern with, at the same time, low cross-polarized radiation as well. As a result, the feeding waveguide should present the smallest possible cross-section defined by the cut-off of the two fundamental modes (i.e.,  $TE_{11h}$  and  $TE_{11v}$ ) and a relatively low initial reflection coefficient (i.e., around -15 dB). Given the fact that there was an opportunity to explore two manufacturing techniques and, therefore, fabricate two antennas, we decided to design the second antenna with a quad-ridged feeding waveguide. Since ridged waveguides present lower cut-off compared to classical hollow waveguides, smaller cross-sections of the former can be considered. As a result, for a given frequency, ridged-waveguides provide a wider-beamwidth radiation pattern compared to the case of a hollow waveguide.

The total antenna was optimized for  $S_{11} < -18$  dB, directivity above 0 dBi over a solid angle of  $|\theta| > \pm 80^{\circ}$  (i.e., a minimum total solid angle of 160°), directivity flatness of 0~6 dBi and XPD > 6 dB over the specified solid angle of  $|\theta| > \pm 80^{\circ}$ . The frequency bandwidth for this case was around 2%. The total antenna design was finalized after the design and inclusion of a single-port

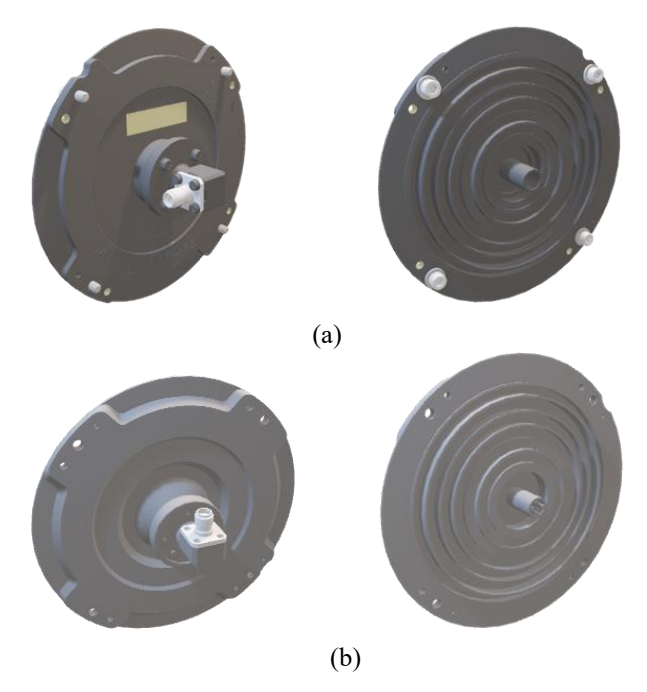


Fig. 1. CAD model of the two choke-ring horn antennas: (a) Conventional manufacturing model and (b) Hybrid manufacturing (the choke-ring horn in additive manufacturing and the septum feeder in milling) model.

septum polarizer, similar to the one referred to [31]. After the finalization of the total design, a sensitivity analysis of the total structure was performed. This showed that the antennas present an acceptable sensitivity for manufacturing tolerances up to  $20{\sim}30$  µm. The total size of the antenna in Fig. 1(a) is  $107{\times}107{\times}44$  mm<sup>3</sup> and of the antenna in Fig. 1(b) is  $107{\times}107{\times}48$  mm<sup>3</sup>.

## III. PROTOTYPING AND MEASUREMENTS

#### A. Prototyping

The two prototypes of the choke-ring horn antennas are shown in Fig. 2. Each antenna consists of two building blocks: the radiating part (choke-ring horn) and the feeding part (septum polarizer). Last, an SMA 2.9 connector is used as a coaxial interface. As explained above, the septum feeder, which is the same for both antennas, is fabricated in conventional milling, a well-established and highly reliable manufacturing technique. The difference between the two antenna elements lies on the radiating part (choke-ring horn), where the first is a machined element [Fig. 2(a)] and the second is a 3D-printed in SLM element [Fig. 2(b)]. The mass of both antennas is lower than 100g.

## B. Measurements

The measurements of the two antenna prototypes have been performed into the compact range spherical near field multi-probe scanner for antenna pattern measurements chamber by MVG StarLab. The method

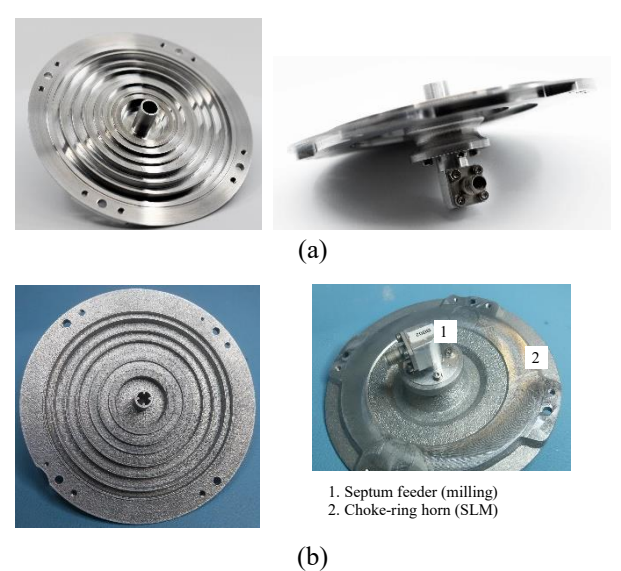


Fig. 2. Prototypes of the two fabricated choke-ring horn antennas: (a) Conventional manufacturing prototype and (b) Hybrid manufacturing prototype.

employed is the so-called indirect measurement technique which is based on Huygens' Principle. This demonstrates that it is possible to reconstruct the electromagnetic field in any location of the space from the measurement of the tangential field on a closed surface surrounding the radiating sources. In simple terms, this technique applies a Near-Field to Far-Field (NF to FF) transformation through appropriate spherical wave expansion operations. The peak gain accuracy (or measurement uncertainty) varies as a function of the AUT operating frequency and peak realized gain value. The total range is between  $\pm 0.3 \sim \pm 1.5$  dB. In the case of 30 GHz and low realized gain (around 6 dBi) the measurement uncertainty as prescribed by MVG's technical datasheet is around  $\pm 0.9$  dB.

Fig. 3 shows the simulated and measured reflection coefficient of the antenna prototype in milling. The two curves indicate that the measurements and simulations agree to a good extent. A frequency shift of around 500 MHz is observed as the principal difference and is attributed to manufacturing tolerances. The measured  $S_{11}$  remains below -18 dB over 29.5~30 GHz.

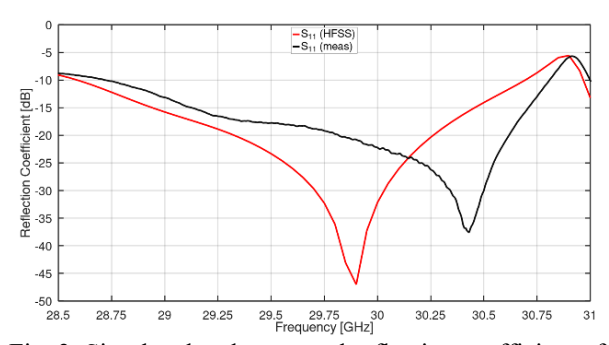


Fig. 3. Simulated and measured reflection coefficient of the antenna prototype in milling.

Figs. 4 to 5 show the radiation performance of the antenna prototype in milling. The antenna presents copolar radiation between 0 to 5.5 dBi and minimum XPD above 5 dB over  $|\theta| \le 80^{\circ}$  and 29.5 to 30 GHz. The front-to-back ratio is above 20 dB. Measurements present less fluctuations over the azimuthal plane which

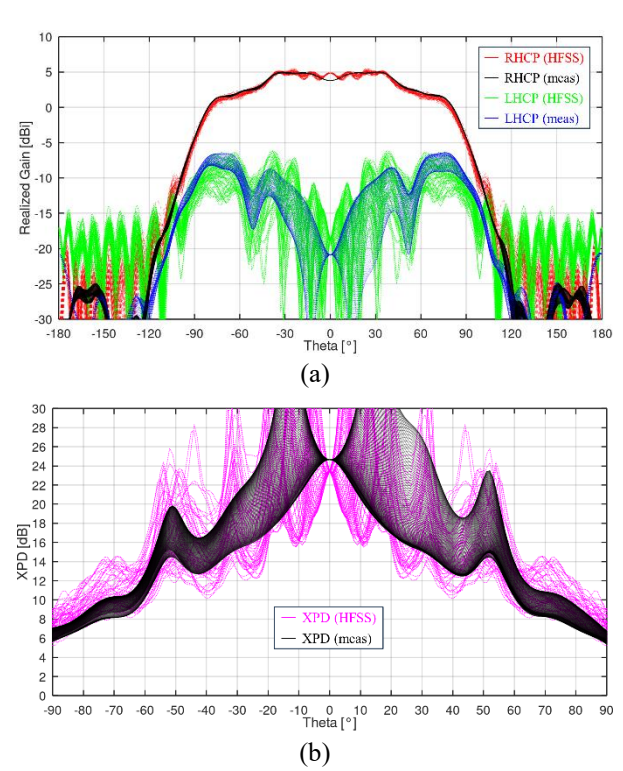


Fig. 4. Radiation performance of the antenna prototype in milling at the central frequency of 29.75 GHz ( $\varphi = 0^{\circ}:5.625^{\circ}:180^{\circ}$ ): (a) RHCP and LHCP radiation patterns and (b) XPD.

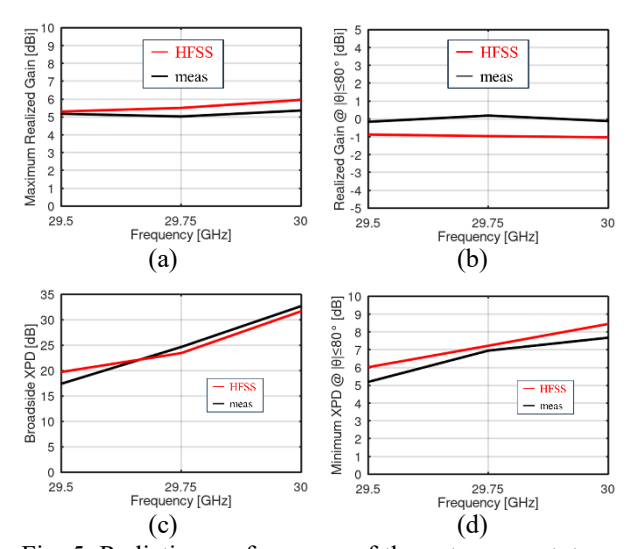


Fig. 5. Radiation performance of the antenna prototype in milling across frequency: (a) maximum realized gain, (b) minimum realized gain over  $|\theta| \le 80^{\circ}$ , (c) broadside XPD and (d) minimum XPD over  $|\theta| \le 80^{\circ}$ .

is attributed to the interpolation of StarLab between sampled measurements of its probes as well as nonidealities at simulations and measurements.

Fig. 6 shows the simulated and measured reflection coefficient of the antenna prototype in hybrid manufacturing. A good agreement between simulations and measurements is observed. A frequency shift of around 700 MHz is observed and is attributed to manufacturing tolerances which now relate also to the additive manufacturing of the choke-ring part. The measured  $S_{11}$  remains below -16 dB over  $29.5 \sim 30$  GHz. Figs. 7 to 8 show the radiation performance of the antenna in hybrid manufacturing. The co-polar radiation lies between -0.5 to 6 dBi and the minimum XPD above 5 dB over  $|\theta| \leq 80^{\circ}$  and 29.5 to 30 GHz.

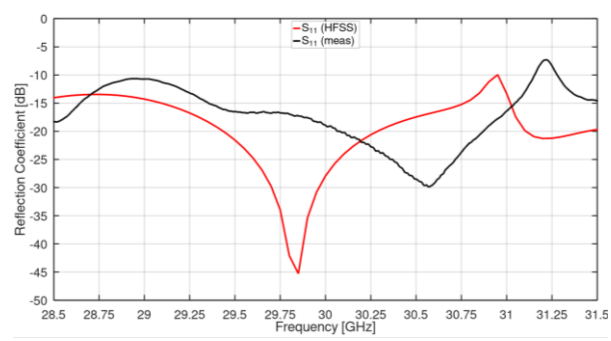


Fig. 6. Reflection coefficient of the antenna prototype in hybrid manufacturing.

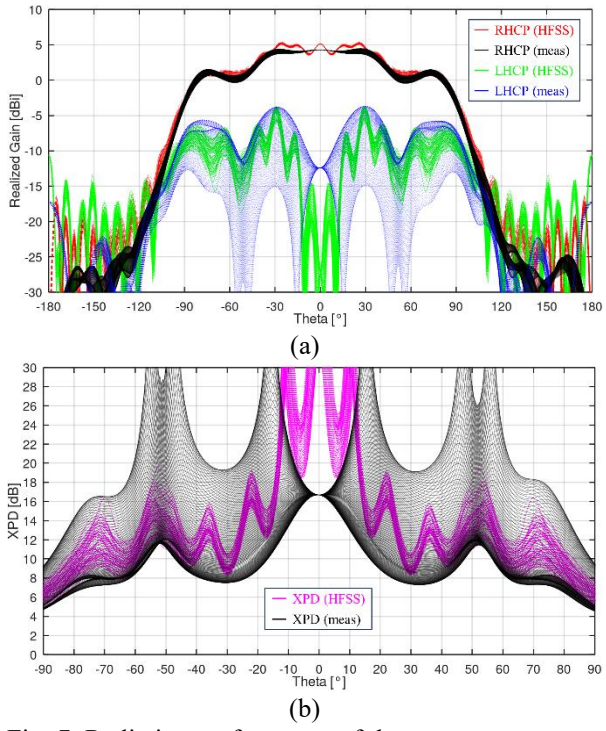


Fig. 7. Radiation performance of the antenna prototype in hybrid manufacturing at the central frequency of 29.75 GHz ( $\varphi = 0^{\circ}$ :5.625°:180°): (a) RHCP and LHCP radiation patterns and (b) XPD.

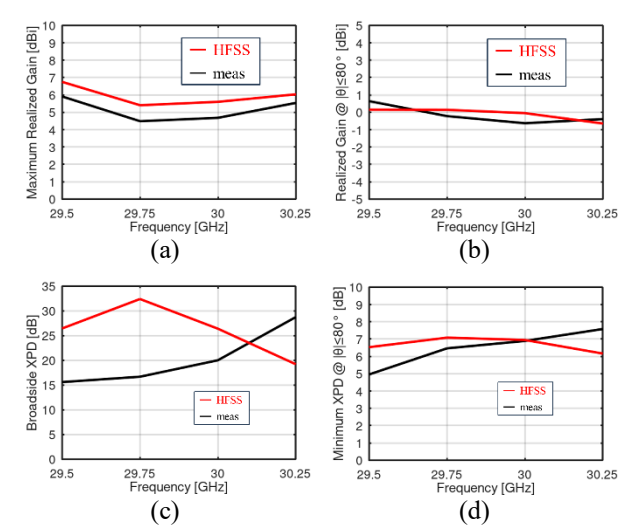


Fig. 8. Radiation performance of the antenna prototype in hybrid manufacturing vs frequency: (a) maximum realized gain, (b) minimum realized gain over  $|\theta| \le 80^{\circ}$ , (c) broadside XPD and (d) minimum XPD for  $|\theta| \le 80^{\circ}$ .

From Figs. 8(c) and 8(d) we can see that the frequency shift is also depicted in the radiation performance of the antenna. Although the performance of this antenna is slightly degraded over the elevation range of  $|\theta| \le 80^{\circ}$ , it is underlined that owing to the quad-ridged feeding waveguide, the antenna presents a broader radiation pattern extending up to  $|\theta| \le 85^{\circ}$  where the realized gain remains above -0.5 dBi (0 dBi in simulations).

## IV. ON-PLATFORM ANALYSIS

This section provides the simulation of the antenna on a 12U satellite platform model. This allows us to monitor the antenna's sensitivity in terms of radiation performance against the presence of a satellite platform. Fig. 9 depicts the setup of the on-platform analysis. The simulation was performed by CST's time domain solver. A Tx and an Rx antenna have been mounted on the platform, with both antennas operating in RHCP. The simulation setup included a total number of 500 million mesh cells, while the total simulation time was 17h on a workstation with an Intel(R) Xeon(R) Gold 6330 CPU @ 2.00GHz and 256 Gb of RAM.

Although not shown for sake of brevity, the S-parameters remain identical between the on-platform and standalone cases. Moreover, the coupling between the two antennas is below -110 dB in Tx-band and -60 dB in Rx-band.

Figs. 10(a) and 10(b) show the simulated 3-D RHCP and LHCP realized gain radiation patterns of the on-platform analysis for the Rx antenna (worst-case), respectively. The hemispherical radiation performance with relatively low cross-polarized level is clearly depicted here. Figs. 10(c) and 10(d) show the simulated RHCP realized gain radiation patterns and the XPD patterns over  $\theta$  for the four principal azimuthal planes (0°:45°:135°  $\varphi$ -cuts).

Although, the central frequency of 29.75 GHz is shown here, the results are rather similar for the two rest frequency points.

The antenna presents coherent radiation performance for the two cases, meaning with and without the presence of the 12U satellite platform over the bandwidth. A slight

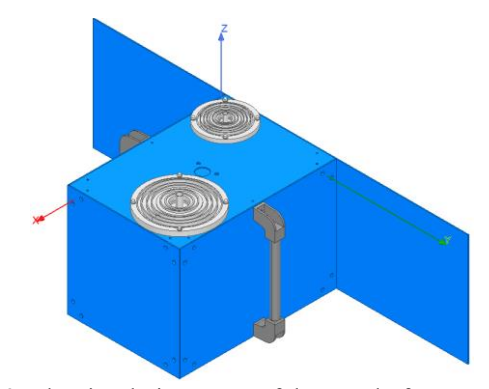


Fig. 9. The simulation setup of the on-platform analysis.

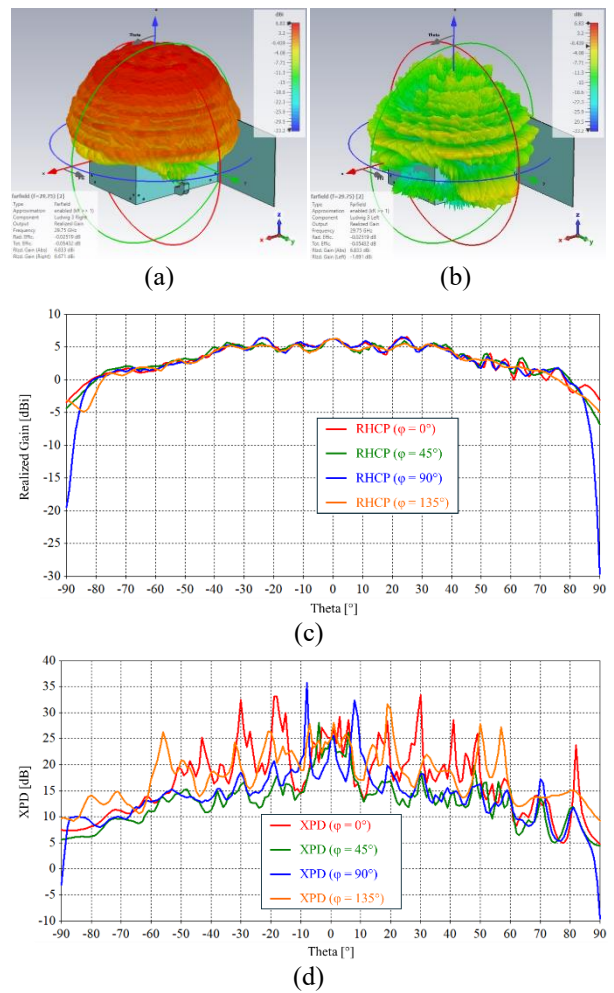


Fig. 10: Simulated realized gain radiation patterns of the on-platform analysis (setup in Fig. 9): (a) 3-D RHCP 29.75 GHz, (b) 3-D LHCP 29.75 GHz, (c) RHCP 29.75 GHz (0°:45°:135°  $\varphi$ -cuts) and (d) XPD 29.75 GHz (0°:45°:135°  $\varphi$ -cuts).

degradation both in the co-polar radiation pattern and the XPD around  $+60^{\circ}$  to  $+80^{\circ}$  of the elevation range  $\theta$  is observed. The Tx antenna's radiation is, as expected, more insensitive against the platform. The current study is going to be experimentally characterized at a later stage, with measurements of the developed antennas on a real satellite platform.

### V. CONCLUSIONS

This work presents the development of two choke-ring horn antennas operating in the Ka-band. Conventional milling and combination with SLM have been selected as manufacturing solutions. Robust radiation performance over  $|\theta| \le 80^{\circ}$  has been achieved. The 3D-printed prototype presents slightly shifted performance owing to manufacturing tolerances. On-platform simulations of the first antenna model showed rather insensitive RF performance, which is a reassuring point for the realistic case of mounting the antenna elements on a real satellite platform where the presence of adjacent components might influence the antennas' performance.

#### VI. REFERENCES

- [1] A. . Modenini and B. Ripani, "A Tutorial on the Tracking, Telemetry, and Command (TT&C) for Space Missions," *IEEE Commun. Surv. Tutor.*, vol. 25, no. 3, pp. 1510-1542, 2023.
- [2] E.-c. Choi, J. W. Lee and T.-K. Lee, "Modified S-Band Satellite Antenna With Isoflux Pattern and Circularly Polarized Wide Beamwidth," *IEEE Antennas Wireless Propag. Lett.*, vol. 12, pp. 1319-1322, 2013.
- [3] Y.-X. Sun, K. W. Leung and K. Lu, "Broadbeam Cross-Dipole Antenna for GPS Applications," *IEEE Trans. Antennas Propag.*, vol. 65, no. 10, pp. 5605-5610, Oct. 2017.
- [4] L. Guo and K. W. Leung, "Compact Linearly and Circularly Polarized Unidirectional Dielectric Resonator Antennas," *IEEE Trans. Antennas Propag.*, vol. 64, no. 6, pp. 2067-2074, Jun. 2016.
- Y. He and Y. Li, "Dual-Polarized Microstrip Antennas With Capacitive via Fence for Wide Beamwidth and High Isolation," *IEEE Trans. Antennas Propag.*, vol. 68, no. 7, pp. 5095-5103, Jul. 2020.
- [6] H. Yang, Y. Fan and X. Liu, "A Compact Dual-Band Stacked Patch Antenna With Dual Circular Polarizations for BeiDou Navigation Satellite Systems," *IEEE Antennas Wireless Propag. Lett.*, vol. 18, no. 7, pp. 1472-1476, Jul. 2019.
- [7] C. Mu, S. Fang, H. Liu, Z. Wang and S. Fu, "3-D-Printed Dielectric Lens With Cone-Shaped Cavity for Axial Ratio Beamwidth Enhancement of Circularly Polarized Patch Antenna," *IEEE Access*, vol. 7, pp. 105062-105071, 2019.
- [8] Y.-D. Yan, Y.-C. Jiao, C. Zhang, Y.-X. Zhang and G.-T. Chen, "Hemispheric Conformal Wide

- Beamwidth Circularly Polarized Antenna Based on Two Pairs of Curved Orthogonal Dipoles in Space," *IEEE Trans. Antennas Propag.*, vol. 69, no. 11, pp. 7900-7905, Nov. 2021.
- [9] A. Adams, R. Greenough, R. Wallenberg, A. Mendelovicz and C. Lumjiak, "The quadrifilar helix antenna," *IEEE Trans. Antennas Propag.*, vol. 22, no. 2, pp. 173-178, Mar. 1974.
- [10] Q.-X. Chu, W. Lin, W.-X. Lin and Z.-K. Pan, "Assembled Dual-Band Broadband Quadrifilar Helix Antennas With Compact Power Divider Networks for CNSS Application," *IEEE Trans. Antennas Propag.*, vol. 61, no. 2, pp. 516-523, Feb. 2013.
- [11] J. Zackrisson, "RUAG space activities in the TT&C, GNSS and data-downlink antenna field," in *Proc. 11th Eur. Conf. Antennas Propag.* (EuCAP'17), Mar. 2017, pp. 529-533.
- [12] H. Liu, M. Shi, S. Fang and Z. Wang, "Design of Low-Profile Dual-Band Printed Quadrifilar Helix Antenna With Wide Beamwidth for UAV GPS Applications," *IEEE Access*, vol. 8, pp. 157541-157548, 2020.
- [13] G. Minatti, S. Maci, P. De Vita, A. Freni and M. Sabbadini, "A Circularly-Polarized Isoflux Antenna Based on Anisotropic Metasurface," *IEEE Trans. Antennas Propag.*, vol. 60, no. 11, pp. 4998-5009, Nov. 2012.
- [14] F. Caminita, E. Martini, G. Minatti, M. Sabbadini and S. Maci, "Low-Profile Dual-Polarized Isoflux Antennas for Space Applications," *IEEE Trans. Antennas Propag.*, vol. 69, no. 6, pp. 3204-3213, Jun. 2021.
- [15] E. Arnaud *et al.*, "Compact Isoflux X-Band Payload Telemetry Antenna With Simultaneous Dual Circular Polarization for LEO Satellite Applications," *Antennas Wireless Propag. Lett.*, vol. 19, no. 10, pp. 1679-1683, Oct. 2020.
- [16] R. Ravanelli, C. Iannicelli, N. Baldecchi and F. Franchini, "Multi-objective optimization of an isoflux antenna for LEO satellite down-handling link," in *Proc. 18th Int. Conf. Microw., Radar Wireless Commun.*, Jun. 2010, pp. 1-4.
- [17] N. Chahat, L. R. Amaro, J. Harrell, C. Wang, P. Estabrook and S. A. Butman, "X-Band Choke Ring Horn Telecom Antenna for Interference Mitigation on NASA's SWOT Mission," *IEEE Trans. Antennas Propag.*, vol. 64, no. 6, pp. 2075-2082, Jun. 2016.
- [18] M. Kilian, C. Hartwanger, A. Schinagl-Weiß and M. Schneider, "X-band downlink antenna characterised by isoflux gain mask," in *Proc. 11th German Microw. Conf.*, 2018, pp. 21–24.
- [19] C. Stoumpos, N. J. G. Fonseca, G. Branger, Q. Lamotte, M. Romier and N. Capet, "Design of a Dual-Band Dual-Polarized Choke-Ring Horn Antenna for TT&C Applications in Ka-Band," in *Proc. 19th Eur. Conf. Antennas Propag.* (EuCAP'25), Mar. 2017, pp. 1-5.

- [20] P. Brachat, "Sectoral pattern synthesis with primary feeds," *IEEE Trans. Antennas Propag.*, vol. 42, no. 4, pp. 484-491, April 1994.
- [21] O. A. Peverini, M. Lumia, G. Addamo, G. Virone and N. J. G. Fonseca, "How 3D-Printing Is Changing RF Front-End Design for Space Applications," *IEEE J. Microw.*, vol. 3, no. 2, pp. 800-814, April 2023.
- [22] L. Wu, H. Chu, D. Cao, S. Peng and Y. Guo, "3-D Printed Antenna Subsystem With Dual-Polarization and its Test in System Level for Radiometer Applications," *IEEE Access*, vol. 8, pp. 127856-127865, 2020.
- [23] M. J. Veljovic and A. K. Skrivervik, "Circularly Polarized Axially Corrugated Feed Horn for CubeSat Reflectarray Applications," in *Proc. 14th Eur. Conf. Antennas Propag. (EuCAP'20)*, Mar. 2020, pp. 1-5.
- [24] I. Agnihotri and S. K. Sharma, "Design of a 3D Metal Printed Axial Corrugated Horn Antenna Covering Full Ka-Band," *IEEE Antennas Wireless Propag. Lett.*, vol. 19, no. 4, pp. 522-526, April 2020.
- [25] A. Sharma and C. Carpenter, "Additive Manufactured Antenna for NASA's Interstellar Mapping and Acceleration Probe (IMAP)," in *Proc. United States Nat. Committee URSI Nat. Radio Sci. Meeting (USNC-URSI NRSM)*, Jan. 2023, pp. 3–4.
- [26] S. S. Hesari *et al.*, "Axially Corrugated Feed Horn for the Next Generation Very Large Array (ngVLA) Band-5 Receiver," *IEEE Open J. Antennas Propag.* (early access)
- [27] C. Menudier et al., "Additive manufacturing of microwave antennas up to 60 GHz," in Proc. Int. Conf. Electromagn. Adv. Appl. (ICEAA), Verona, Italy, 2017, pp. 885–887. 2017 International Conference on Electromagnetics in Advanced Applications (ICEAA), Sep. 2017, pp. 1551-1554.
- [28] A. Reinhardt, M. Möbius-Labinski, C. Asmus, A. Bauereiss and M. Höft, "Additive Manufacturing of 300 GHz Corrugated Horn Antennas," in *Proc. IEEE MTT-S Int. Microw. Workshop Ser. Adv. Mater. Processes RF THz Appl.*, 2019, pp. 40–42.
- [29] M. Tafertshofer, M. Binder and E. Biebl, "3D-Printing of Slanted Corrugated Horn Antennas for the E-Band," *Prog. Electromagnet. Res. M*, Vol. 128, pp. 127-134, 2024.
- [30] H.-H. Viskum, "CHAMP—The dedicated design tool for rotationally symmetric horns and reflector terminals," in *Proc. IEEE Antennas Propag. Soc. Int. Symp. (APSURSI'13)*, Jul. 2013, pp. 2325–2326.
- [31] M. Fallahzadeh, H. Aliakbarian, A. Haddadi and S. Radiom, "Beam shaping of X-band stepped choke ring antenna for LED satellite applications," *IEEE Aerosp. Electron. Syst. Mag.*, vol. 33, no. 10, pp. 34–39, Oct. 2018.